

RECENT RESULTS FOR STRESS-INTENSITY FACTORS SOLUTIONS FOR CRACKS GROWING OUT OF FASTENER HOLES

Anisur Rahman
Drexel University
Department of Materials Engineering
Philadelphia, PA 19104, USA
Telephone: (215) 895-2382
Telefax: (215) 895-6684

John G. Bakuckas, Jr., Catherine A. Bigelow, and Paul W. Tan
FAA William J. Hughes Technical Center
AAR-430
Atlantic City International Airport, NJ 08405, USA

ABSTRACT

To predict crack growth and residual strength of riveted joints subjected to widespread fatigue damage (WFD), accurate stress and fracture analysis of corner and surface cracks emanating from a rivet hole are needed. To address this need, an effort is made to expand the existing database of three-dimensional stress-intensity factor solutions. The solutions are obtained using the finite element method and by applying a global-intermediate-local hierarchical approach. The stress-intensity factors were determined at different locations along the countersunk hole. A wide range of crack shapes is considered representing typical damage scenario in an aircraft fuselage. The stress-intensity factors are normalized as boundary correction factors. Three different loading scenarios are considered: far-field tension, far-field bending, and wedge loading. The results presented in this paper focus on cracks under far-field bending. In general, the relative magnitude of the stress-intensity factor at a point in the crack front is proportional to its distance from the hole boundary. However, this is locally influenced by the presence of stress-raisers such as points along the countersunk hole where the geometry changes abruptly and the relative magnitude of the load transferred in the vicinity of the point on the crack front. All these local effects tend to increase the stress-intensity factor.

INTRODUCTION

To improve the airworthiness of the aging aircraft fleet, ongoing research activities are aimed at developing and implementing advanced fatigue and fracture mechanics concepts into the damage tolerance analysis. These activities include methods to predict the onset

of widespread fatigue damage (WFD). The Industry Committee on Widespread Fatigue Damage was formed to implement a long-term cooperative program to develop a common understanding of the WFD phenomena and to improve the identification of likely locations and assessment methodologies. One of the objectives of the Federal Aviation Administration's National Aging Aircraft Research Program is to develop the methodology to predict crack initiation, crack growth rates, and residual strengths of aircraft structures susceptible to WFD. Among the 16 possible locations susceptible to WFD, identified by the Industry Committee on WFD, the riveted lap splice joint has been identified as one of the critical locations on an aircraft. Widespread fatigue damage at riveted lap splice joints is usually in the form of multiple cracks emanating from the stress concentrations in the rivet holes. To reliably predict crack growth rates and fracture strengths of riveted joints subjected to WFD, accurate stress-intensity factor (SIF) solutions of corner and surface cracks at a rivet hole are needed.

Exact closed-form SIF solutions for cracks in three-dimensional solids are often lacking for complex configurations, such as countersunk rivet holes. Therefore, approximate solutions must be used. Over the past two decades, considerable effort has been placed on developing computationally efficient methods to provide highly accurate SIF solutions for cracks in three-dimensional bodies. These methods include the conventional finite element method (FEM) [1-4], the finite element alternating method (FEAM) [5-7], the boundary element method (BEM) [8, 9], and the three-dimensional weight function method (WFM) [10, 11]. With advances in pre- and post-processors, computer hardware, and improvements in equation solvers, timesavings are being realized in both geometry development and analysis of complex models. With computational tools in place, much needed SIF solutions required for damage tolerance assessments of cracked rivet holes can be obtained.

Some work has been done to generate SIF solutions for cracks in countersunk rivet holes [4, 12, 13]. However, many gaps exist in available SIF solutions and further work is required, particularly for solutions under bending and wedge loading. The objective of this study is to develop SIF solutions for cracks at countersunk rivet holes to expand on the currently available solution database. Configurations representing typical countersunk holes in aircraft structural joints were analyzed under tension, bending, and wedge-loading conditions. The crack size, crack shape, and crack location were varied to represent typical experimental observations. A global-intermediate-local (GIL) hierarchical approach, based on the finite element method, was used to obtain the solutions.

In this paper, a subset of the solutions is presented focusing on cracks under bending load. Deformation due to bending is inherent to a fuselage containing a longitudinal crack. Bending is introduced at crack faces due to crack bulging. The bulging crack produces higher strains at the outer edge compared to the inner edge. However, at a lap splice joint, secondary bending is introduced at the lap joint due to offset between the inner and outer skin at the lap joint area. The secondary bending results in higher strains at the inner surface of the outer skin which is opposite to that observed over most of the fuselage. This anomalous behavior is due to the offset between the inner skin and outer

skin. It has been analytically explained by Müller [14] and has also been experimentally verified at the FAA FASTER facility. In this test, a full-scale fuselage panel containing a lap joint is pressured up to 16 psi. The lap joint area is instrumented as shown in Figure 1. A representative verification result is shown in Figure 2 [15]. The results show the micro-strain (μ -strain) at Strain Gages 1T and 1B. These are back-to-back strain gages at the critical outer rivet row and aligned along the hoop direction. The results show consistently that the strain reading of gage “SG 1T” is lower than at gage “SG 1B”. Thus, higher strain is along the inner surface of the outer skin.

CONFIGURATIONS AND LOADINGS

The crack configurations that were analyzed are shown in Figure 3. Cracks nucleating from three locations were considered. The locations are the corner, the knee, and the lip. At the corner location, the straight shank portion of the rivet hole intersects the inner surface of the skin. The straight and inclined section of the countersunk rivet hole meet at the knee. In the lip region, the inclined portion of the rivet hole intersects the outer face of the skin. Three crack shapes (a/c ratio) were considered: 0.4, 0.7, and 2.0. The following crack depth ratios (a/t ratio) were used: 0.2, 0.3, and 0.4. The height of the straight shank portion of the countersunk hole was assumed to be half of the thickness of the plate, and the radius of the straight shank was taken as twice the thickness. The bending load was applied as a linearly varying far-field tension. Two load cases were considered. In the first load case, the tension load was assumed to be S_b at the inner surface and zero at the outer surface. In the second load case, the tension load was assumed to be zero at the inner surface and S_b at the outer surface. The first load case represents bending at the critical outer rivet row of the outer skin in a lap joint. The second load case represents the bending at rivet holes at lap joints where the inner skin is riveted to the doubler [14, 15].

DEFINITION OF BOUNDARY CORRECTION FACTOR

In this work, the stress-intensity factor results are normalized to boundary correction factors. The boundary correction factor is defined for mode I stress-intensity factor (K_I) at any location along the crack front under bending as:

$$F_b\left(\frac{a}{t}, \frac{a}{c}, \frac{h}{t}, \frac{R}{t}, \theta\right) = \frac{K_I}{S_b \sqrt{\frac{\pi a}{Q}}} \quad (1)$$

The crack dimensions, a and c , and the physical angle, θ , are defined in Figure 3. The shape factor, Q , is given by the square of the complete elliptic integral of the second kind. The integral can be approximated by [16]:

$$Q = \begin{cases} 1 + 1.464 \left(\frac{a}{c} \right)^{1.65} & \text{for } \frac{a}{c} \leq 1 \\ 1 + 1.464 \left(\frac{c}{a} \right)^{1.65} & \text{for } \frac{a}{c} > 1 \end{cases} \quad (2)$$

GLOBAL-INTERMEDIATE-LOCAL HIERARCHICAL APPROACH

The global-intermediate-local (GIL) hierarchical finite element approach, illustrated in Figure 6 and established and verified by Bakuckas [17], was used to obtain the boundary correction factors for countersunk rivet holes. The commercially available finite element program ABAQUS 5.8 [18] was used for the analysis. In the first step (global level) of the GIL approach, an analysis of the plate subjected to the prescribed loading conditions and using a relatively coarse mesh was conducted. For the cases analyzed here, due to symmetry in the geometry and loading, one quadrant of the plate was modeled. The global model typically contained 1200 20-noded brick elements.

In the next stage (intermediate level), an analysis of the area of interest using a more refined mesh is conducted; in these cases, the area of interest was the higher stress gradient region near the hole. The intermediate model typically consisted of 5000 20-noded brick elements. The boundary conditions for the intermediate model were taken from the global model using the submodeling features in ABAQUS.

In the final stage (local level), an analysis is conducted that is even more focused on the region of interest, which was the region immediately around the crack front. The highly refined local mesh typically consisted about 7000 20-noded brick elements. The boundary conditions for the local model were taken from the intermediate model again using the submodeling features in ABAQUS.

From local models, the J-integral was calculated along the crack front using the equivalent domain integral method (EDIM). Assuming a plane strain elastic material response in the direction of crack propagation, the mode I SIF K_I , at any point along the crack front, can be calculated from the J-integral as:

$$K_I = \sqrt{\frac{JE}{1-\nu^2}} \quad (3)$$

Here, J is the value of J-integral, E is the Modulus of Elasticity, and ν is the Poisson's ratio.

It should be noted that, for the small cracks, the full GIL approach (three levels) was required. For the larger crack sizes, a two-level global-local hierarchical approach was sufficient to obtain sufficiently accurate results.

RESULTS AND DISCUSSIONS

Stress-intensity factors were obtained for cracks at the three locations along the countersunk hole. For each location, three crack shapes (a/c ratios) and three crack depths (a/t ratios) were considered. Finally, two different bending modes were considered; thus a total of 54 solutions were obtained. Typical results are presented to illustrate the effect of crack shape, crack location, and bending mode on the stress-intensity factor.

EFFECT OF CRACK SHAPE

Figure 7 depicts the effect of crack shape on the mode I SIF for corner cracks. These results are for bending load case 1 where the bending load is applied by a linearly varying tension in which the load is maximum at the inner surface. Three different crack shapes are shown ($a/c = 0.4, 0.7$, and 2.0). All cracks have the same a/t ratio. In the plot, the stress-intensity factor is normalized as the boundary correction factor and plotted as a function of the physical angle. The physical angle is zero where the crack front meets the inner surface and is 90° where the crack front intersects the straight shank of the hole.

For the two crack shapes with $a/c < 1.0$, the boundary correction factor increased as one moves along a crack front from the inner surface to the intersection of the crack front with the straight shank portion of the hole. At a given physical angle θ , as one moves from one crack shape to another, the boundary correction factor is proportional to the distance from the corner of the straight shank and the inner surface of the plate. Since a/t ratio is constant, all the cracks presented in this plot have the same a value and different c values. a is measured along the hole axis and c is measured along the radial direction. Thus, the crack front for $a/c = 0.4$ starts further away from the corner than the crack front for $a/c = 0.7$. However, they both intersect the straight shank portion of the hole boundary at the same a value. Thus the boundary correction factor for $a/c = 0.4$ is lower at $\theta = 0^\circ$ than $a/c = 0.7$, but, as one moves along the crack fronts, the boundary correction factor for both the crack shapes increases and converges to the same value at $\theta = 90^\circ$.

For the crack front with $a/c = 2.0$, the behavior is quite different. At $\theta = 0^\circ$, this crack front is the closest to the corner and consequently has a high value for the boundary correction factor. However, as one moves along the crack front the boundary correction factor decreases almost monotonically. Such a phenomenon has been observed for similar cracks under tension [7]. This can be attributed to the fact that, as one moves along this crack front from $\theta = 0^\circ$ to $\theta = 90^\circ$, one moves further and further from the corner. This is opposite to what happens when one moves along a crack front with $a/c < 1$ where the distance from the corner increases as one moves along the crack front in a similar manner.

EFFECT OF CRACK LOCATION

Figure 8 shows the boundary correction factors for a crack with a/c ratio of 0.4 and a/t ratio of 0.2 at three different locations along the rivet hole. The loading mode is again

load case 1 as described in the previous section. The crack locations are shown in Figure 4. The boundary correction factor is plotted as a function of the physical angle θ for all three locations. For the corner crack, θ is measured along the crack front from the inner surface to the straight shank portion of the rivet hole. Thus, the value of θ is between 0° and 90° , with $\theta = 0^\circ$ at the inner surface and $\theta = 90^\circ$ at the straight shank. For the knee crack, θ is measured along the crack front from the straight shank portion to the inclined portion of the rivet hole. At this location, the value of θ is between 0° and 130° , with $\theta = 0^\circ$ where the crack front intersects the straight shank and $\theta = 130^\circ$ at the other end of the crack front where it intersects the countersunk portion of the rivet hole. Finally for the lip crack, θ is measured along the crack front from the outer skin to the countersunk portion of the rivet hole. In this case, θ spans 140° with $\theta = 0^\circ$ at the outer skin and $\theta = 140^\circ$ at the countersunk region.

Thus, in interpreting the results depicted in Figure 8, one should recognize that each of the curves representing a different location, spans a different range along the θ axis. For the corner crack, the boundary correction factor increases monotonically as one moves along the crack front from the inner surface to the straight shank portion of the rivet hole. However, when the crack is at the knee, the behavior is quite different. Here the crack front starts close to the knee, which is a stress raiser due to abrupt geometry change. Thus, the boundary correction factor starts from a high value. However, as one moves along the crack front, one moves away from the stress raisers and the boundary correction factor decreases. It reaches a minimum at $\theta = 90^\circ$, the point on the crack front that is farthest from the knee. Then, as one moves further along the crack front, one returns to the inclined section of the rivet hole and consequently the boundary correction factor increases. One can observe by the shape of the plot that a crack at this location will tend to grow at the edges until it becomes a breakthrough crack. Finally, for the crack at the lip, one observes that, overall, the boundary correction factors are very small, since the load level in this region and the consequent stress gradient are very low in this region.

EFFECT OF CRACK DEPTH

Figure 9 depicts the effect of crack depth for cracks at the knee with a/c ratio of 0.4. Three a/t ratios are considered. All three curves lie close together, and hence, one can conclude that a/t ratio does not have significant effect on the boundary correction factor at this location. One can, however, observe subtle differences between the curves. Observing closely, one can see that, at the two ends of the crack, the boundary correction factors are influenced by the proximity of the crack to the corner and/or the knee of the rivet hole. Thus, $a/t = 0.4$ has the highest boundary correction factor at $\theta = 0^\circ$, since it is closest to the corner. At $\theta = 140^\circ$, when the crack front intersects the inclined portion of the rivet hole, the trend is reversed and $a/t = 0.2$ has the highest value of boundary correction factor, since it is closest to the knee.

EFFECT OF BENDING MODE

Two different bending loads were considered in this study. In the first case, defined by load case 1, the bending was assumed to be concave outward and was introduced by applying a linear tensile load which was maximum at the inner surface and zero at the outside surface. The second loading case was applied by assuming a concave inward bending. In this mode, the tensile load was applied so that it was zero at the inner surface and maximum at outside surface. Thus, load case 1 produces maximum stresses in the corner region of the rivet hole and minimum stresses at the lip region. On the other hand, load case 2 produced maximum stresses in the lip region and minimum stresses in the corner region. The effect of the bending load was mainly on the magnitude of the boundary correction factor. The shape of the plot was more dependent on the location and the a/c ratio of the crack. This is illustrated in Figure 10, where, for a corner crack with $a/c = 0.4$ and $a/t = 0.2$, the boundary correction factors are plotted. At this location, load case 1 results in the largest correction factors and load case 2 produces small values of the boundary correction factors. The plot shows that, while both the curves for the two loading mode have similar shape, load case 1 results in much higher values for boundary correction factor. The magnitude is directly related to the stress level in the crack region. In the results for the corner crack depicted in Figure 10, the load case 1 results in a larger stress level in this area and, consequently, larger values for the boundary correction factor. In the lip region, load case 1 produces the smaller stresses compared to load case 2. Thus, one would expect that the effect of the loading mode would be reversed for cracks at the lip. Since both the load cases produce about the same level of stresses in the knee area, one would expect changing the load case to have minimal effect on cracks at the knee.

CONCLUDING REMARKS

Three-dimensional stress-intensity factor solutions for cracks at countersunk rivet holes were obtained using the finite element method. Since both types of bending are observed in an aircraft fuselage, two bending loads were considered. These results along with previously obtained results for tension and wedge loading provide the elementary solutions that can be combined together to obtain stress-intensity factors for more complex loading.

ACKNOWLEDGEMENTS

This research was supported in part by an Aviation Research Grant (00-G-030) from the Federal Aviation Administration. The computational effort was partially supported by National Computational Science Alliance and used the Silicon Graphics Origin 2000 Distributed Shared Memory System at University of Illinois at Urbana-Champaign.

REFERENCES

1. Raju, I. S. and J. C. Newman, Jr., "Stress Intensity Factors for Two Symmetric Cracks," in *Fracture Mechanics*, C. W. Smith, ed, Philadelphia, PA, American Society of Testing Materials, 1979.
2. Packard, A. C., "Stress-Intensity Factors for Cracks with Circular and Elliptic Crack Fronts - Determined by 3d Finite Element Method," Rolls Royce Limited, May 1980.
3. Tan, Paul W., Raju, I. S., Shivakumar, K. N., and Newman, J. C., Jr., "Evaluation of Finite Element Models and Stress-Intensity Factor for Surface Cracks Emanating from Stress Concentrations," in *Surface Crack Growth: Models, Experiments, and Structures*, ASTM STP 1060, Philadelphia, PA, American Society of Testing Materials, pp. 34-48, 1990.
4. Gosz, M. and Moran, B., "Stress-Intensity Factors for Elliptical Cracks Emanating from Countersunk Rivet Holes," *DOT Report - DOT/FAA/AR-95/111*, April 1998.
5. Nishioka, T. and Alturi, S.N., "Analytical Solution for Elliptical Cracks and Finite Element Alternating Method for Elliptical Surface Cracks Subjected to Arbitrary Loadings," *Engineering Fracture Mechanics*, Vol. 17, pp. 247-268, 1983.
6. Nishioka, T. and Alturi, S.N., "An Alternating Method for Analysis of Surface Flawed Aircraft Structural Components," *AIAA Journal*, Vol. 21, pp. 749-757, 1983.
7. Tan, Paul W., Bigelow, Catherine A., O'donoghue, P.E., and Alturi, S.N., "Stress-Intensity Factor Solutions for Cracks at Countersunk Rivet Holes under Uniaxial Tension," *DOT Report - DOT/FAA/CT-93/68*, February 1994.
8. Heliot, J., Lebbens, R. C., and Pellissier-Tanon, A., "Semi-Elliptical Surface Cracks Subjected to Stress Gradients," in *Fracture Mechanics*, ASTM STP 667, C. W. Smith, ed, Philadelphia, PA, American Society of Testing Materials, pp. 341-364, 1979.
9. Cruse, T. A., "Application of Boundary-Integral Equation Method to Three-Dimensional Stress Analysis," *Computers and Structures*, Vol. 3, pp. 509-527, 1994.
10. Zhao, W., Newman, J. C., Jr., Sutton, M. A., Wu, X. R., and Shivakumar, K. N., "Analysis of Corner Cracks at Hole by a 3-D Weight Function Method With Stresses From Finite Element Method," National Aeronautics and Space Administration Langley Research Center, Hampton, VA, *NASA Technical Memorandum- 110144*, 1995.

11. Zhao, W., Wu, X. R., and Yan, M.G., "Weight Function Method for Three-Dimensional Crack Problems," *Engineering Fracture Mechanics*, Vol. 34, pp. 593-607, 1989.
12. Rahman, Anisur, Bakuckas, J. G., Jr., Bigelow, Catherine A., and Tan, Paul W., "Boundary Correction Factors for Elliptical Surface Cracks Emanating From Countersunk Rivet Holes," *AIAA Journal*, Vol. 38, pp. 2171-2175, 2000.
13. Rahman, Anisur, Bakuckas, John G., Jr., Bigelow, Catherine A., and Tan, Paul W., "Boundary Correction Factors for Elliptic Surface Cracks Emanating From Countersunk Rivet Holes under Tension, Bending and Wedge Loading Conditions," *DOT Report - DOT/FAA/AR-98/37*, March 1999.
14. Muller, Richard Paul Gerhard, "An Experimental and Analytical Investigation on the Fatigue Behaviour of Fuselage Riveted Lap Joints," *Ph.D Dissertation*, Faculty of Aerospace Engineering, Delft University of Technology, Delft, The Netherlands, 1995.
15. Ahmed, A., Bakuckas, J. G., Jr., Bigelow, C. A., Tan, P.W., Awerbuch, J., Lau, A., and Tan, T., "Initiation and Distribution of Fatigue Cracks in Fuselage Lap Joint Curved Panel," presented at Fifth Joint NASA/FAA/DoD Conference on Aging Aircraft, Kissimmee, FL, 2001.
16. Murakami, Y., *Stress Intensity Factors Handbook*, 1st ed. Oxford [Oxfordshire] , New York, Pergamon, 1987.
17. Bakuckas, John G., Jr., "Comparison of Boundary Correction Factor Solutions for Two Symmetric Cracks in a Straight-Shank Hole," *DOT Report - DOT/FAA/AR-98-36*, April 1999.
18. *ABAQUS*, Ver 5.8. Hibbitt, Karlsson, and Sorenson (HKS), Pawtucket, RI 02860, 1998.

FIGURES

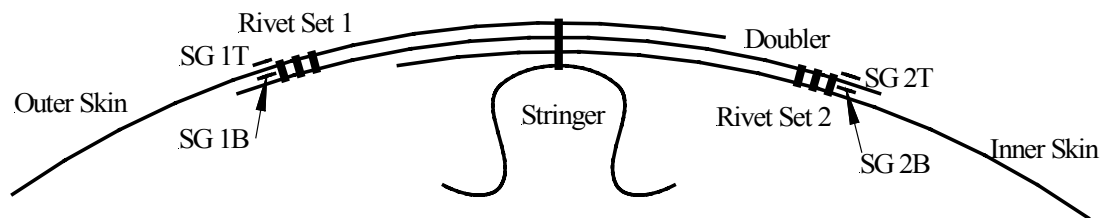


Figure 1. Schematic of Longitudinal Lap Joint Tested on FASTER with Strain Gage Positions Marked

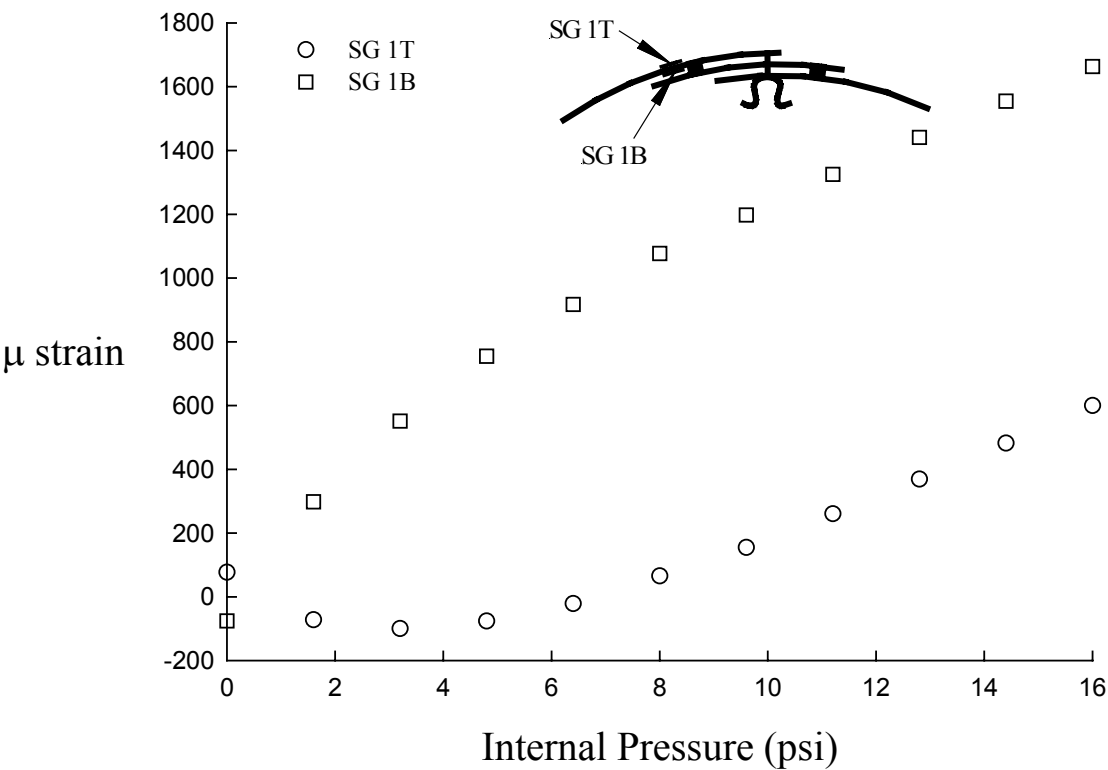


Figure 2. Strain Survey Results From FASTER Test

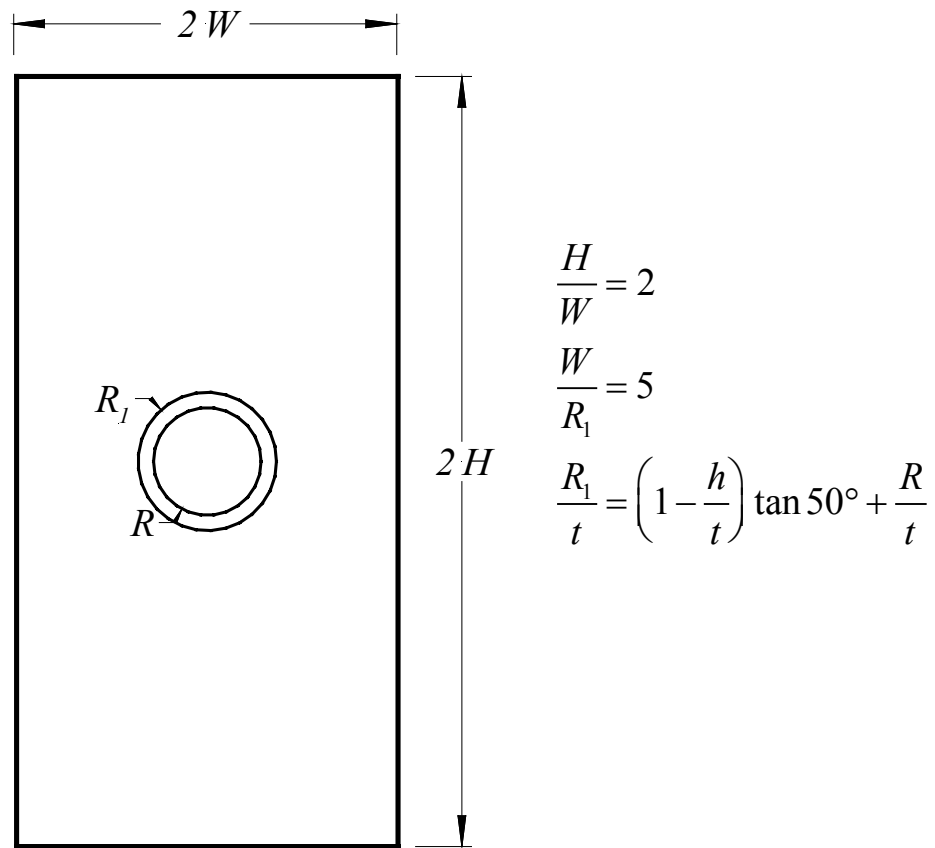


Figure 3. Specimen Configuration

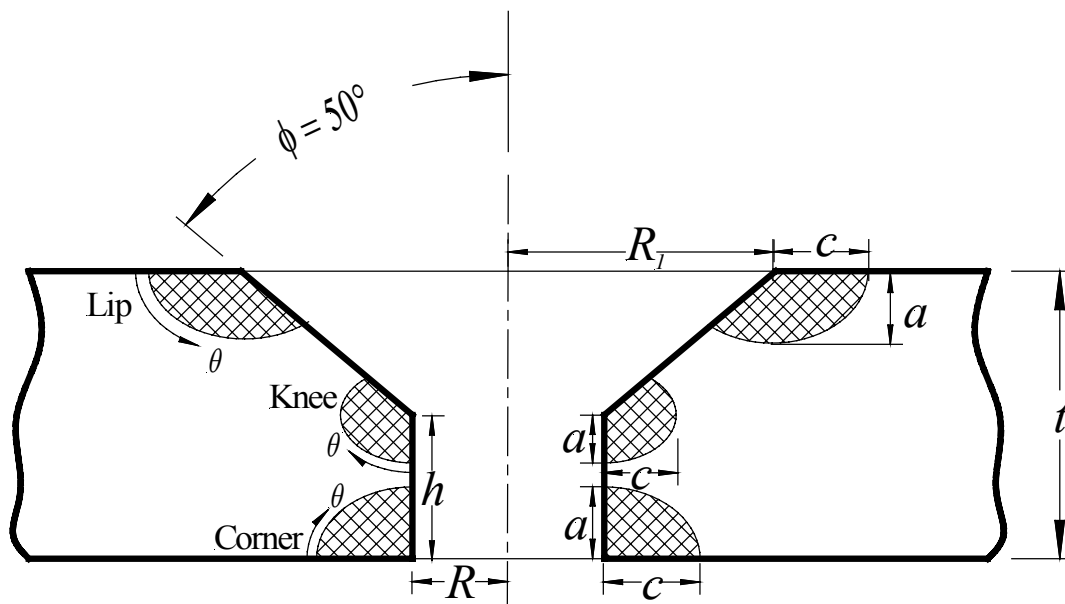


Figure 4. Crack Locations and Crack Configurations

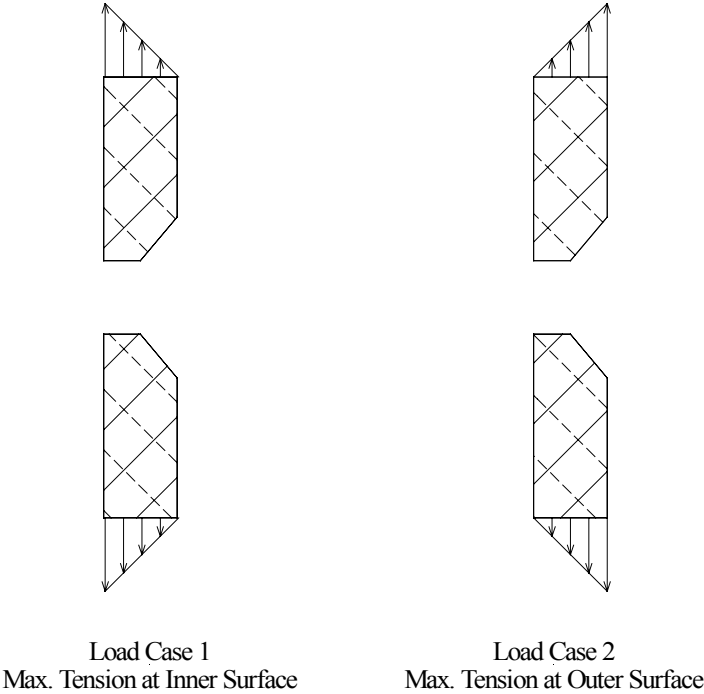


Figure 5. Bending Loading Modes

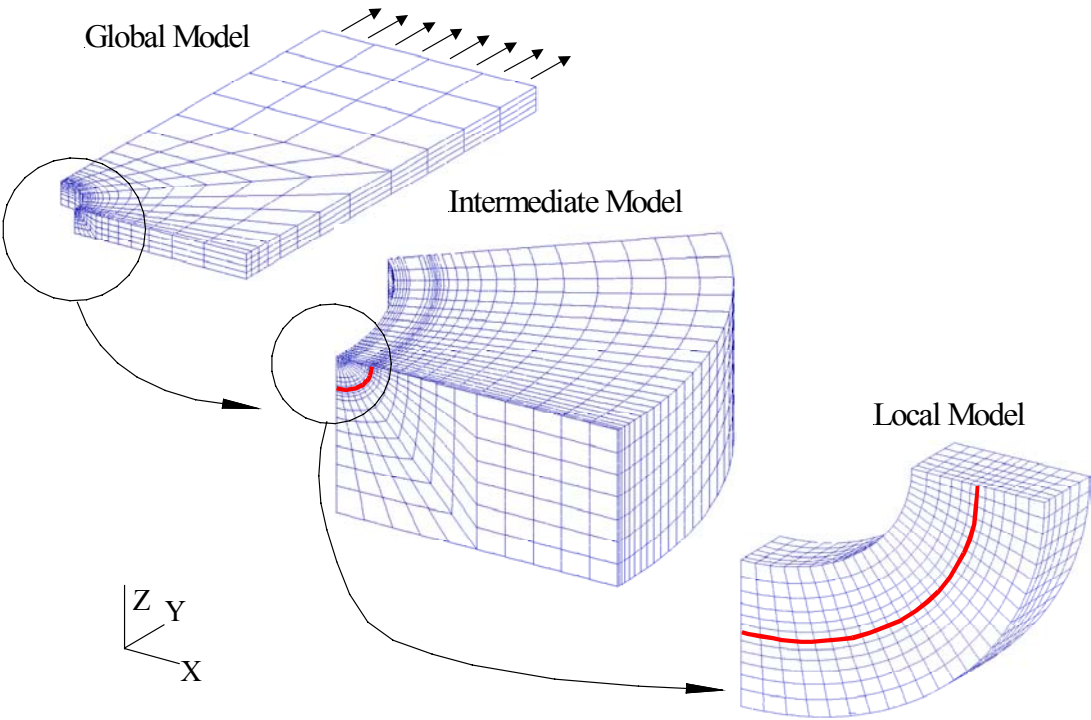


Figure 6. Global-Local-Intermediate approach

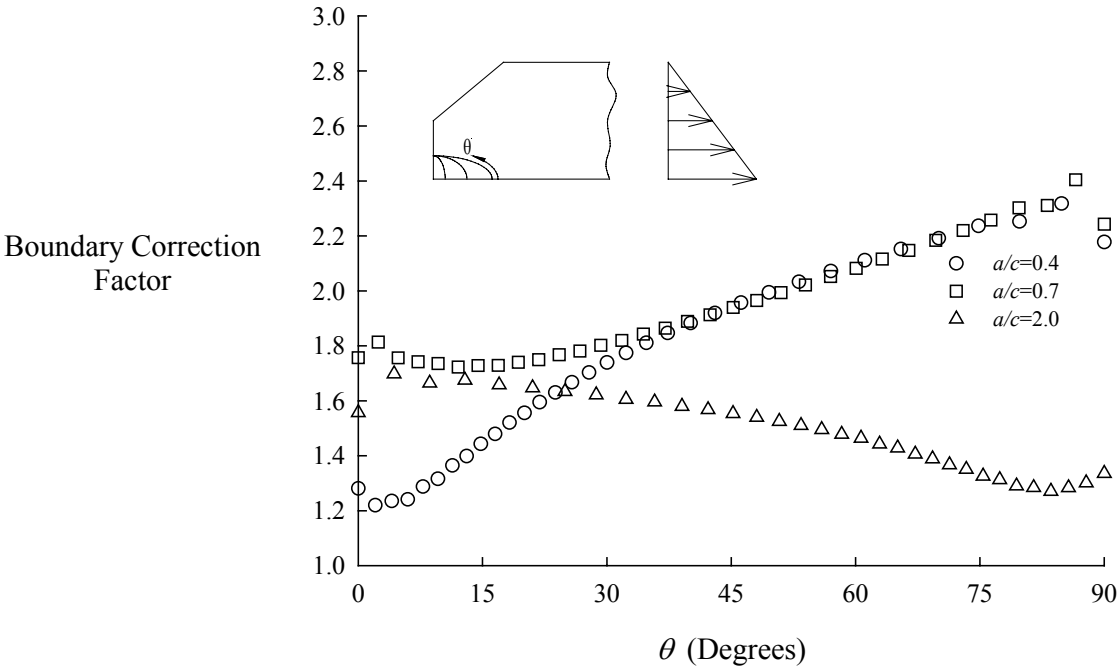


Figure 7. Effect of Crack Shape on the Mode I Stress-Intensity Factor

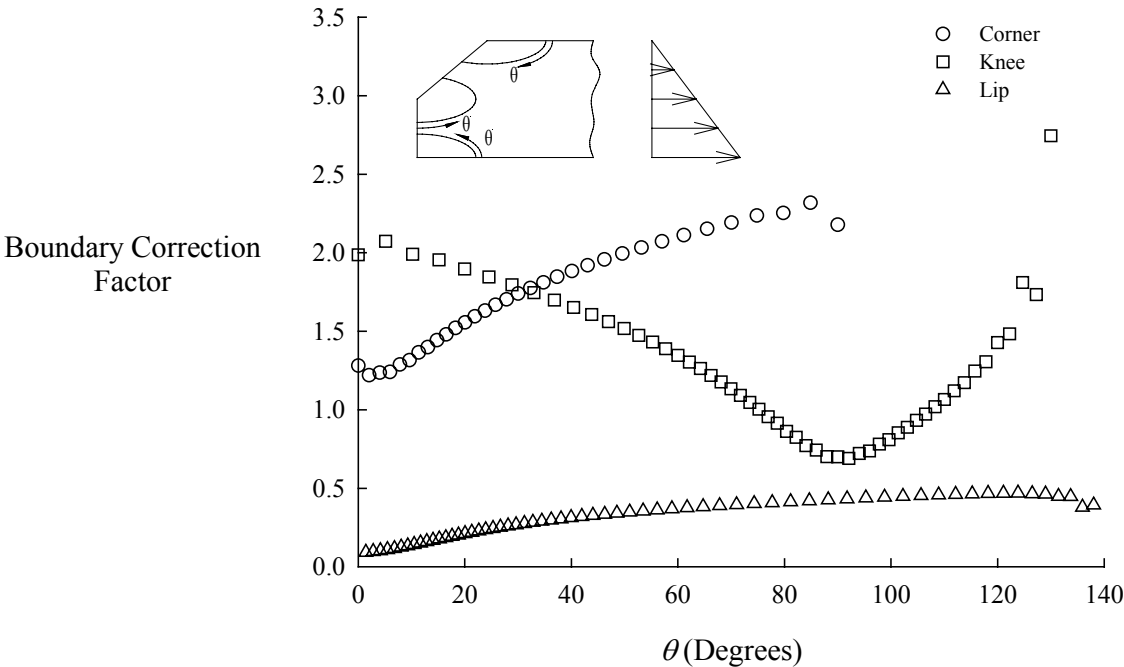


Figure 8. Effect of Crack Location on the Mode I Stress-Intensity Factor

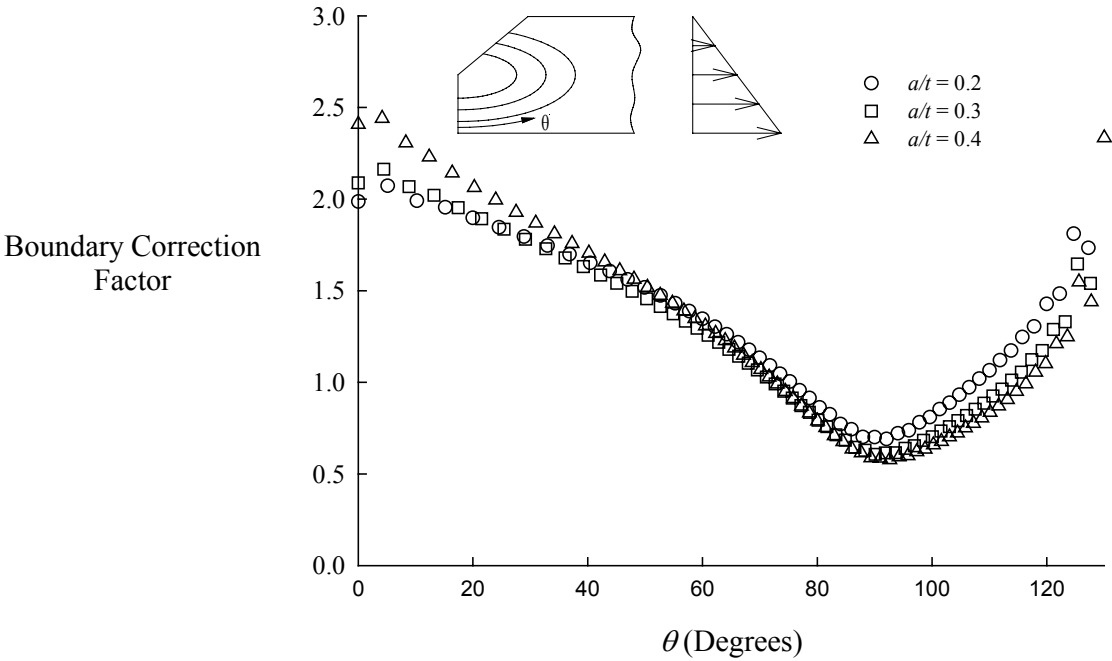


Figure 9. Effect of Crack Depth on the Mode I Stress-Intensity Factor

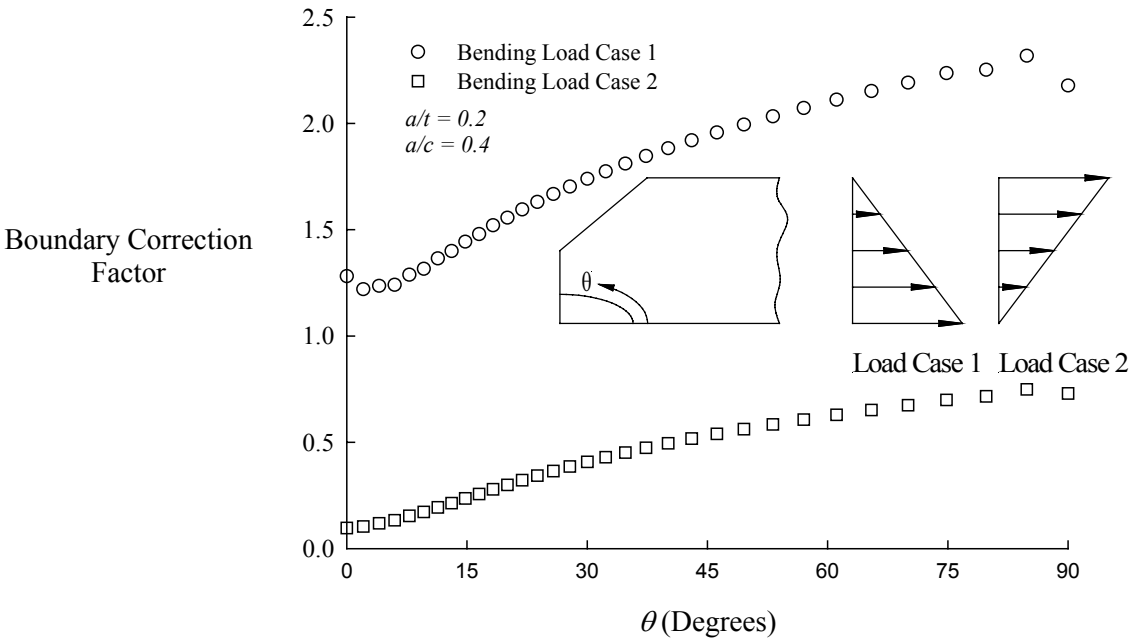


Figure 10. Effect of Bending Load on the Mode I Stress-Intensity Factor